arXiv:cond-mat/0103289v1 [cond-mat.mtrl-sci] 14 Mar 2001

Phase-Field Formulation for Quantitative Modeling of Alloy Solidification

Alain Karma
Physics Department and Center for Interdisciplinary Research on Complex Systems, Northeastern University, Boston, Massachusetts 02115
(March 7, 2001)

A phase-field formulation is introduced to simulate quantitatively microstructural pattern formation in alloys. The thin-interface limit of this formulation yields a much less stringent restriction on the choice of interface thickness than previous formulations and permits to eliminate non-equilibrium effects at the interface. Dendrite growth simulations with vanishing solid diffusivity show that both the interface evolution and the solute profile in the solid are well resolved.

05.70.Ln, 81.30.Fb, 64.70.Dv, 81.10.Aj

The phase-field approach has emerged as a method of choice to simulate microstructural evolution during solidification [1–8]. This approach has the well-known advantage that it avoids to explicitly track a sharp boundary by smearing the interface region over some thickness $\sim W$. However, it has the disadvantage that it is hard to use quantitatively. This is because it is often computationally too stringent to choose W small enough to resolve the desired sharp-interface limit of the phase-field model, even on computers of today. This is especially true for small growth rates where the scale of the microstructure is typically several orders of magnitude larger than the microscopic capillary length d_0.

Progress has recently been made to overcome this difficulty by using a "thin-interface" analysis of the phase-field model [3–5] where W is assumed small compared to the scale of the pattern, but not smaller than d_0. For the standard symmetric model (with equal thermal conductivities in the solid and liquid), Karma and Rappel (KR) have shown that this thin-interface limit yields two essential benefits [3]. Firstly, it maps onto the standard set of sharp-interface equations that one obtains in the classical sharp-interface limit where $W/d_0 \to 0$, but yields a much less stringent restriction on W/d_0 that renders the computations tractable. Secondly, it makes it possible to eliminate interface kinetic effects by a specific choice of phase-field model parameters.

These two properties combined have made this thin-interface limit ideally suited to model dendritic growth in pure materials quantitatively at low undercooling when used in conjunction with efficient numerical algorithms [6,7]. However, how to extend these results in a useful way to the more general case where the two phases do not have symmetrical properties has remained an open challenge. Using a distinct thin-interface analysis, Almgren showed that the two-sided model with unequal thermal conductivities maps onto a modified set of sharp-interface equations that is plagued by finite interface thickness effects [4]. These include (i) a temperature jump across the interface, (ii) an interface stretching correction to the heat conservation condition at the interface (Stefan condition) also found previously in [9], and (iii) a surface diffusion correction to the same condition.

The same effects plague the thin-interface limit of existing phase-field models of alloy solidification [2,8] and make them inadequate to model quantitatively the low growth rate regime of experimental relevance. In alloys, (i) translates into a chemical potential jump across the interface associated with the well-known effect of solute trapping [10], and (ii) and (iii) modify the mass conservation condition at the interface. Here, I present a phase-field formulation of alloy solidification that makes it possible to eliminate *simultaneously* all three effects. Furthermore, I demonstrate that it yields the same computational benefits as the thin-interface limit of the symmetric model [3] for dendritic growth.

For clarity of exposition, I first discuss the thin-interface limit of a simpler model that describes an idealized binary alloy with parallel liquidus and solidus slopes, and which reduces to the standard Hele-Shaw flow problem [11] in its Laplace limit. I then consider a realistic dilute alloy model with unequal slopes that reduces to the former model in the limit where the partition coefficient $k \to 1$. The equations of the first model are

$$\tau \partial_t \phi = W^2 \nabla^2 \phi - \partial_\phi \left[f(\phi) + \lambda\, g(\phi)\, u \right], \tag{1}$$

$$\partial_t c + \vec{\nabla} \cdot \vec{j} = 0, \tag{2}$$

where c is the concentration defined as the mole fraction of B in a binary alloy of A and B,

$$\vec{j} = -\Delta c_0\, D\, q(\phi) \vec{\nabla} u - a_t\, W\, \Delta c_0\, \partial_t \phi\, \vec{\nabla}\phi / |\vec{\nabla}\phi|, \tag{3}$$

and

$$u \equiv c/\Delta c_0 + h(\phi)/2 - (c_{s0} + c_{l0})/(2\Delta c_0) \tag{4}$$

is a dimensionless measure of the departure of the chemical potential from its equilibrium value with $u = 0$ in equilibrium. c_{s0} (c_{l0}) are the equilibrium concentrations in the solid (liquid) at a fixed temperature T_0, $\Delta c_0 \equiv c_{l0} - c_{s0}$, $f(\phi) = -\phi^2/2 + \phi^4/4$ is a double well function with the minima $\phi = \pm 1$ corresponding to the solid ($+1$) and liquid (-1), $g(\phi)$ is an odd function of ϕ with $g(\pm 1) = \pm 1$ and vanishing first and second derivatives $g'(\pm 1) = g''(\pm 1) = 0$, and $h(\phi)$ is an odd function of ϕ with $h(\pm 1) = \pm 1$ that can be chosen independently of $g(\phi)$ for non-variational dynamics [3].

The above model reduces to the symmetric model for the choice $q(\phi) = 1$ and $a_t = 0$. In this case, the thin-interface limit of this model maps onto the Stefan problem defined by: $\partial_t u = D\nabla^2 u$ in both phases, the Stefan condition $V = -D(\partial_n u|^+ - \partial_n u|^-)$, where V is the interface velocity and $\partial_n u|^\pm$ is the normal gradient of u on the solid $(-)$ and liquid side $(+)$ of the interface, and the velocity-dependent Gibbs-Thomson condition

$$u = -d_0\kappa - \beta V, \tag{5}$$

where

$$d_0 = a_1 W/\lambda, \quad \text{and} \quad \beta = a_1\left[\tau/(W\lambda) - a_2 W/D\right]. \tag{6}$$

The expressions for the coefficients a_1 and a_2 are identical to those derived by KR [3] and interface kinetics can be eliminated ($\beta = 0$) by choosing $\lambda = D\tau/(a_2 W^2)$.

Next, for the alloy case, $q(\phi)$ must now be chosen to vary from $q(-1) = 1$ in the liquid to $q(+1) = D_{\rm solid}/D$ in the solid. I consider explicitly the one-sided limit where $D_{\rm solid}/D \to 0$, but the results also extend to the more realistic case where $D_{\rm solid}/D \ll 1$. The essential new term that yields the desired thin interface limit is the *anti-trapping* mass current that corresponds to the second term on the right-hand-side of equation (3), and is only non-vanishing in the diffuse interface region. It produces a solute flux from the solid to the liquid along the direction normal to the interface that counter-balances the trapping current associated with the jump of chemical potential across the interface: $\Delta u \equiv u^+ - u^-$, where $u^\pm$ correspond to the liquid $(+)$ and solid $(-)$ sides of the interface. Thus the anti-trapping current makes it possible to eliminate this jump while still leaving enough freedom to choose the other functions in the model to eliminate the corrections to the mass conservation condition. Repeating the analyses of KR [3] and Almgren [4], I obtain that Δu vanishes if $F^+ = F^-$, where

$$F^\pm = \int_0^{\pm\infty} d\eta\left[p(\phi_0(\eta)) - p(\mp 1)\right], \tag{7}$$

and

$$p(\phi_0) = \left(h(\phi_0) - 1 + a_t\sqrt{2}\,(1-\phi_0^2)\right)/q(\phi_0). \tag{8}$$

In the above definitions, $\phi_0(\eta) = -\tanh(\eta/\sqrt{2})$ is the equilibrium phase-field profile, where η is a coordinate that runs normal to the interface scaled by W, and I have used the identity $\partial_\eta\phi_0 = -(1-\phi_0^2)/\sqrt{2}$. Next, the mass conservation condition has the form

$$V = -D\,\partial_n u|^+ - c_1 W\kappa V - c_2 W D\,\partial_s^2 u \tag{9}$$

where $c_1 \equiv H^+ - H^-$, $c_2 \equiv Q^+ - Q^-$, and

$$H^\pm = \int_0^{\pm\infty} d\eta\left[h(\phi_0(\eta)) - h(\mp 1)\right], \tag{10}$$

$$Q^\pm = \int_0^{\pm\infty} d\eta\left[q(\phi_0(\eta)) - q(\mp 1)\right]. \tag{11}$$

The second and third term on the right-hand-side of equation (9) represent the solute redistribution due to stretching the interface and by diffusion along its arclength s, respectively. These two terms appear, equivalently, at two successive orders in the thin interface limit considered by KR, or both at second order in the distinct thin-interface limit considered by Almgren [4].

In summary, one is left with three conditions to satisfy: (i) $F^+ = F^-$ (chemical potential jump), (ii) $H^+ = H^-$ (stretching), and (iii) $Q^+ = Q^-$ (surface diffusion). It is actually possible to satisfy two of these three conditions simultaneously within the standard phase-field formulation without the anti-trapping current. For example, with $a_t = 0$ in equation (3), the choice $h(\phi) = 1 - (1-\phi)^2/2$ and $q(\phi) = (1-\phi)/2$ satisfy (i) and (iii), but not (ii), and it is also possible to satisfy (i) and (ii) but not (iii). However, test simulations show that with either c_1 or c_2 non-vanishing, the morphological stability of the interface that sets the initial scale of the pattern becomes significantly altered for computationally tractable choices of W [12], which is also easy to check analytically by repeating the standard Mullins-Sekerka analysis with the modified boundary condition (9). Similarly, it can be shown that solvability theory predictions for the dendrite tip become modified. Consequently, all three conditions must be satisfied to lift the restriction on W.

With the anti-trapping current present, one is now free to make the simplest choices $h(\phi) = \phi$ and $q(\phi) = (1-\phi)/2$ that satisfy $H^+ = H^-$ and $Q^+ = Q^-$, respectively. By choosing $a_t = 1/(2\sqrt{2})$, one can then reduce the function $p(\phi_0)$ to the simple form $p(\phi_0) = \phi_0 - 1$ that satisfies $F^+ = F^-$ (and a non-vanishing amount of trapping can also be obtained by varying a). Remarkably, with these choices, the thin interface limit of the one-sided model produces a velocity-dependent Gibbs-Thomson condition that is *identical* to the one of the symmetric model. Consequently the expressions for a_1 and a_2 that determine d_0 and β are the same as in Ref. [3]: $a_1 = I/J$ and $a_2 = (K + JF)/(2I)$ where $I = \int_{-\infty}^{+\infty} d\eta(\partial_\eta\phi_0)^2$, $J = g(-1) - g(+1)$, $F \equiv F^\pm = \sqrt{2}\ln 2$, and

$$K = \int_{-\infty}^{+\infty} d\eta\,\partial_\eta\phi_0(\eta) g'(\phi_0(\eta)) \int_0^\eta d\xi\,\phi_0(\xi), \tag{12}$$

where I have defined $g'(\phi) \equiv \partial_\phi g(\phi)$. It also follows that the standard Hele-Shaw flow problem with an infinite viscosity contrast [11] can be simulated by taking the limit $\partial_t u \to 0$ of the present phase-field model.

Consider now the standard one-sided dilute alloy model defined by the set of equations

$$\partial_t c = D\nabla^2 c, \tag{13}$$

$$c_l(1-k)V = -D\partial_n c|^+, \tag{14}$$

$$c_l/c_l^0 = 1 - (1-k)d_0\,\kappa \tag{15}$$

where $d_0 = \gamma T_M/[L|m|(1-k)c_l^0]$ is the chemical capillary length, T_M is the melting temperature, L is the latent

heat of melting, m is the liquidus slope, $k = c_s/c_l$ is the partition coefficient where c_l (c_s) is the concentration on the liquid (solid) side of the interface, and solidification is again assumed to take place isothermally.

To construct a thin interface limit that maps onto the free-boundary problem (13)-(15), I follow the same procedure of adding a local anti-trapping current in order to eliminate the jump of chemical potential together with the other terms. The equations are

$$\tau\partial_t\phi = W^2\nabla^2\phi \, - \partial_\phi \left[f(\phi) + \frac{\lambda}{1-k}\, g(\phi)(e^u - 1) \right], \tag{16}$$

with the same continuity relation (2) as before,

$$\vec{j} = -D\, c\, q(\phi)\vec{\nabla}u \, - \, a_t\, W\, c_l^0(1-k)\, e^u\, \partial_t\phi\, \vec{\nabla}\phi/|\vec{\nabla}\phi|, \tag{17}$$

$$u = \ln\left[\frac{2c/c_l^0}{1+k-(1-k)h(\phi)} \right], \tag{18}$$

and where $g(\phi)$, $h(\phi)$, and $q(\phi)$ obey the same limits at $\phi = \pm 1$. u is again a dimensionless measure of the departure of the chemical potential μ from equilibrium (namely here $u \equiv v_0(\mu - \mu_E)/(RT_0)$ where R is the rare gas constant and v_0 is the molar volume assumed to be constant). The logarithmic dependence of u on c is related to the entropy of mixing in the free-energy density as in previous models [2,8]. The main difference here is again the addition of the anti-trapping mass current. Also, the present thin-interface analysis differs from the analysis of Kim *et al.* [8] that does not consider interface stretching and surface diffusion, and assumes that $q(\phi)$ is constant in the interface region.

The condition for eliminating surface diffusion becomes now $Z^+ = Z^-$, where $Z^\pm = \int_0^{\pm\infty} d\eta\, [M(\eta) - M(\pm\infty)]$ where $M(\eta) \equiv q(\phi_0(\eta))\, c_0(\eta)$, and

$$c_0(\eta) = c_l^0\, [1 + k - (1-k)h(\phi_0(\eta))]\, /2 \tag{19}$$

is the equilibrium concentration profile across a stationary interface. Therefore choosing

$$q(\phi) = \frac{1-\phi}{1+k-(1-k)h(\phi)} \tag{20}$$

satifies this condition. The choices $h(\phi) = \phi$ and $a_t = 1/(2\sqrt{2})$ then make the jump of u and the interface stretching term vanish up to finite corrections that turn out to be small in computations and will be discussed elsewhere. Consequently, the conditions for c on the two sides of the interface have the desired form, $c_l/c_l^0 = 1 - (1-k)d_0\kappa - (1-k)\beta V$ and $c_s = kc_l$ where the expressions for d_0, β, a_1, and a_2 are again identical to those for the symmetric model quoted earlier here. Therefore, β can again be made to vanish. The dilute alloy model is easily shown to reduce to the parallel slope model in the limit $k \to 1$ by making the change of variable $U = (e^u - 1)/(1-k)$. A small solid diffusivity can also be modeled by adding $(1+\phi)D_{\rm solid}/(2D)$ to the right-hand-side of equation (20), which has a negligible effect on the thin-interface limit in typical alloys where solid diffusion is substitutional ($D_{\rm solid}/D \sim 10^{-4}$) [10].

Finally, the model is straightforward to extend to directional solidification with the standard frozen temperature approximation $T(z) = T_0 + G(z - V_p t)$ that yields (for $\beta = 0$) the interface condition

$$c_l/c_l^0 = 1 - (1-k)d_0\kappa - (1-k)(z - V_p t)/l_T, \tag{21}$$

where V_p is the pulling velocity of the sample along the z-axis, $l_T = |m|(1-k)c_l^0/G$ is the thermal length , G is the temperature gradient, and $c_l^0 = c_\infty/k$ where $c_\infty \equiv c(z = +\infty)$. It simply suffices to substitute e^u by $e^u + (1-k)(z - V_p t)/l_T$ in equation (16).

The convergence of the model was examined by carrying out two-dimensional simulations of isothermal dendritic growth. These simulations are directly analogous to the ones carried out previously to test the thin interface limit of the symmetric model [3]. Crystalline anisotropy was included by generalizing equation (16) to a standard anisotropic form

$$\begin{aligned} \tau(\Theta)\, \partial_t\phi = &-\partial_\phi \left[f(\phi) + \frac{\lambda}{1-k}\, g(\phi)(e^u - 1) \right] \\ &+ \vec{\nabla}\cdot(W(\Theta)^2\vec{\nabla}\phi) - \partial_x\left(W(\Theta)W'(\Theta)\partial_y\phi\right) \\ &+ \partial_y\left(W(\Theta)W'(\Theta)\partial_x\phi\right), \end{aligned} \tag{22}$$

where $\Theta \equiv \arctan(\partial_y\phi/\partial_x\phi)$ is the angle between the direction normal to the phase-field interface and the x-axis. As a result, the anisotropic form of d_0 and β become $d_0(\theta) = a_1[W(\theta) + W''(\theta)]/\lambda$ and $\beta(\theta) = a_1\,[\tau(\theta)/(W(\theta)\lambda) - a_2 W(\theta)/D]$ in the interface condition where $a_1 = 0.8839$, and $a_2 = 0.6267$ for the common choice $\partial_\phi g(\phi) = (1-\phi^2)^2$. Furthermore, I chose the standard form of four-fold anisotropy $W(\theta) = W a_s(\theta)$ with $a_s(\theta) = 1 + \epsilon_4 \cos 4\theta$ and made $\beta(\theta)$ vanish by letting $\tau(\theta) = \tau a_s(\theta)^2$ and $\lambda = D\tau/(a_2 W^2)$.

I simulated equations (2) and (22) with $\vec{j}$ and u defined by equations (17) and (18), respectively. I compare the results of the present model with $a_t = 1/(2\sqrt{2})$ and $q(\phi)$ defined by equation (20), to the more standard choice (i.e. similar to previous models) that has no anti-trapping current ($a_t = 0$) and uses the simplest scaled diffusivity function $q(\phi) = (1-\phi)/2$; $h(\phi) = \phi$ and $\partial_\phi g(\phi) = (1-\phi^2)^2$ in both models. The former model has the desired thin-interface limit with local equilibrium at the interface, whereas the latter has both a chemical potential jump and surface diffusion. I used a simple finite-difference Euler method with $\Delta x = 0.4$ and $\Delta t = 0.008$, $W = \tau = 1$, $\epsilon_4 = 0.02$, $k = 0.15$, and the scaled supersaturation $\Omega = (c_l^0 - c_\infty)/[c_l^0(1-k)] = 0.55$ where c_∞ is the initial alloy concentration. In all simulations, the initial condition consisted of a circular seed of radius $r = 22\, d_0$, $u = \ln(1-(1-k)\Omega)$, and c defined by equation (18) that varies from c_∞ in liquid to kc_∞ in solid.

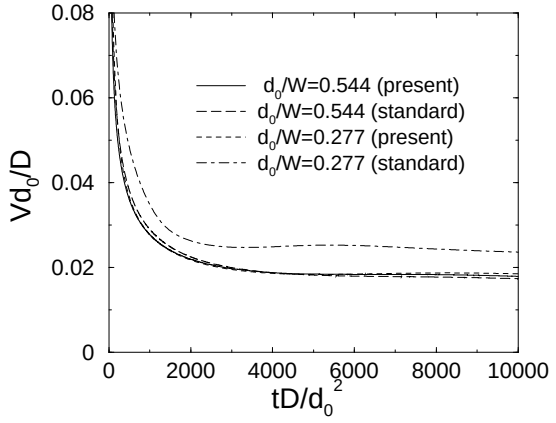

FIG. 1. Plots of scaled dendrite tip velocity Vd_0/D vs scaled time tD/d_0^2 for $a_t = 1/(2\sqrt{2})$ and $q(\phi)$ given by Eq. 20 (present), and $a_t = 0$ and $q(\phi) = (1-\phi)/2$ (standard).

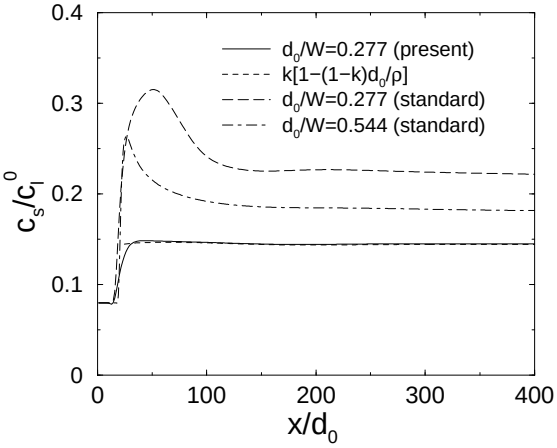

FIG. 2. Plots of solute profiles in the solid along the central dendrite axis, and comparison with the Gibbs-Thomson relation for the present model (short-dash line).

The dimensionless dendrite tip velocity Vd_0/D is plotted vs the dimensionless time tD/d_0^2 for the two models and two different ratios of d_0/W in Fig. 1. Since the simulation time scales $\sim (d_0/W)^5$, the runs with d_0/W twice smaller are ≈ 32 times shorter. Furthermore, I have plotted in Fig. 2 the scaled concentration $c_s(x)/c_l^0$ in the solid vs the scaled position x/d_0 along the central dendrite axis for the two different models. Plots in Figs. 1-2 must superimpose when results are converged. These plots show, as expected, that the present model is well converged in this range of d_0/W that is comparable to the one studied in the symmetric model [3], whereas the standard model is not. This is especially true for the microsegregation profile that is still far from being converged in the latter model, even for the largest ratio $d_0/W = 0.544$. In contrast, this profile is already well converged for a twice smaller ratio in the present model; it agrees, self-consistently, within a few percent with the Gibbs-Thomson relation $c_s(x)/c_l^0 = k[1-(1-k)d_0/\rho]$ where ρ is the dendrite tip radius in the simulation. It will be shown elsewhere that this dramatic difference of convergence for microsegregation is due to the fact that the amount of solute trapped $\sim p \ln p$ for small velocity ($p = WV/D \ll 1$) in the standard model.

The present results demonstrate that the phase-field method can be successfully extended to model quantitatively microstructural pattern formation in alloys with a realistic solid diffusivity. For this important application, it is potentially more advantageous than the level set method [13] since it does not require the explicit computation of the interface velocity. These results also revive the hope to extend the phase-field method to model accurately a wide range of other interfacial patterns with a strong asymmetry between phases.

This research is supported by U.S. DOE Grant No. DE-FG02-92ER45471 and benefited from computer time allocation at NERSC and NU-ASCC. I thank Roger Folch and Mathis Plapp for valuable discussions.

[1] J. B. Collins and H. Levine, Phys. Rev. B **31**, 6119 (1985); J. S. Langer, in *Directions in Condensed Matter*, edited by G. Grinstein and G. Mazenko (World Scientific, Singapore, 1986), p. 164; G. Caginalp and P. Fife, Phys. Rev. B **33**, 7792 (1986).

[2] A. A. Wheeler, W. J. Boettinger, and G. B. McFadden, Phys. Rev. A**45**, 7424 (1992); Phys. Rev. E**47**, 1893 (1993); G. Caginalp and W. Xie, Phys. Rev. E**48**, 1897-1909 (1993); J. A. Warren and W. J. Boettinger, Acta Metall. Mater. A**43**, 689-703 (1995); J. Tiaden, B. Nestler, H. J. Diepers, and I. Steinbach, Physica D **15**, 73 (1998).

[3] A. Karma and W.-J. Rappel, Phys. Rev. E**53**, R3017 (1996); Phys. Rev. E**57**, 4323 (1998).

[4] R. F. Almgren, SIAM J. Appl. Math **59**, 2086 (1999), also considers a distinct thin-interface limit where finite thickness effects appear as higher order corrections in the classical asymptotics where W/d_0 is assumed small.

[5] G. B. McFadden, A. A. Wheeler, and D. M. Anderson, Physica D **154**, 144 (2000).

[6] N. Provatas, N. Goldenfeld, and J. Dantzig, Phys. Rev. Lett. **80**, 3308 (1998); J. Comp. Phys. **148**, 265 (1999).

[7] M. Plapp and A. Karma, Phys. Rev. Lett. **84**, 1740 (2000); J. Comp. Phys. **165**, 592 (2000); A. Karma, Y. H. Lee, and M. Plapp, Phys. Rev. E**61** 3996 (1999).

[8] S.-G. Kim, W. T. Kim, and T. Suzuki, Phys. Rev. E **60**, 7186 (1999).

[9] P. C. Fife and O. Penrose, Electron. J. Diff. Equations **1**, 1 (1995).

[10] W. Kurz and D. J. Fisher, *Fundamentals of solidification* (Trans Tech, Aedermannsdorf, Switzerland, 1992).

[11] P. G. Saffman and G. I. Taylor, Proc. R. Soc. London, Ser. A **245**, 312 (1958). For a different phase-field formulation of this problem with arbitrary viscosity contrast, see R. Folch *et al.*, Phys. Rev. E **60**, 1724 (1999).

[12] R. Folch, A. Karma, and M. Plapp (unpublished).
[13] S. Osher and J. A. Sethian, J. Comp. Phys. **79**, 12 (1988); Y.-T. Kim, N. Goldenfeld, and J. Dantzig, Phys. Rev. E **62**, 2471 (2000).